PAPER

A dielectrophoresis-based microfluidic chip for trapping circulating tumor cells using a porous membrane

IOP Publishing Journal of Micromechanics and Microengineering
J. Micromech. Microeng. **32** (2022) 015008 (9pp) https://doi.org/10.1088/1361-6439/ac3c89

A dielectrophoresis-based microfluidic chip for trapping circulating tumor cells using a porous membrane

Malihe Farasat, Seyede Maede Chavoshi, Atin Bakhshi, Aref Valipour and Majid Badieirostami

MEMS Lab, School of Electrical and Computer Engineering, College of Engineering, University of Tehran, Tehran, Iran

E-mail: m.farasat66@yahoo.com

Received 29 August 2021, revised 19 November 2021
Accepted for publication 23 November 2021
Published 8 December 2021

Abstract

Circulating tumor cells (CTCs) have been widely considered as novel biomarkers for the clinical diagnosis of cancer. CTCs are the cells detached from the parent tumors and shed into the blood stream to initiate tumor metastasis. Although CTCs are rare, their detection in one's blood sample is essential for cancer early diagnosis and for starting the treatment procedure. Here, we introduce a novel method for trapping CTCs using dielectrophores, which effectively employs pores of a replaceable porous membrane as CTC traps. The applied dielectrophoretic force efficiently traps and holds CTCs in a stable position and further enables us to perform various on-chip analysis with them. First, using finite element method, the performance of the system was simulated for different physical conditions. Then, the chip was fabricated and its trapping performance was experimentally validated. Cells were entered into the microchannel and trapped in the pores of a polydimethylsiloxane membrane. The proposed microfluidic chip is capable of detecting rare cells in a large cell population.

Keywords: microfluidics, lab-on-a-chip, CTCs, dielectrophoresis, cell trapping

(Some figures may appear in colour only in the online journal)

1. Introduction

Microfluidics has been a well-received technology for the experimental study of cell biology for almost the past two decades. The significant advantages of this technology include less sample volume consumption, fast response time, and facilitation of single-cell analysis and tracking. Microfluidic chips are extremely useful for single-cell analysis as they can capture and manipulate complex cells and enable us to study these cells in their native fluidic environments without damaging them. Circulating tumor cells (CTCs), shedding from primary malignant tumors and entering into the blood, are considered a major cause of cancer metastasis [1]. CTCs are extremely rare compared to the number of normal blood cells (in the order of 1–10 CTCs per ml of whole blood); hence their early detection is very challenging tough very essential for cancer early diagnosis. Sorting, trapping, and purification of CTCs are essential in many lab-on-a-chip devices having different clinical applications like prognosis, diagnosis, monitoring after treatment, or drug resistance assessment [2–4]. Various methods exist for isolating or trapping CTCs based on their surface proteins, physical size and deformability, and electrical and mechanical characteristics. To name a few of the existing methods, they are antibody-coated microposts [5], size-based separation by microfilters [6], and electrophoresis and acoustophoresis-based cell separation [3, 7–9]. In general, one can classify the reported CTC isolating schemes into two categories: Affinity-based and label-free CTC isolating methods.

Affinity-based methods rely on biomarkers and surface antigens of CTCs, such as epithelial cell adhesion molecule

(EpCAM), to detect and isolate CTCs. CELLSEARCH (Menarini Silicon Biosystems, Huntingdon Valley, PA, USA) [10], the only commercial system approved by the United States Food and Drug Administration (FDA), is a good example of affinity-based systems used for clinical isolation of CTCs in patient's blood samples. It uses magnetic nanoparticles to label CTCs with anti-EpCAM antibodies. Nevertheless, this method is not completely reliable due to the epithelial-to-mesenchymal transition happening in subpopulations of tumor cells, which can cause EpCAM failure to identify aggressive CTCs. Besides, in affinity-based sorting, the cell surface is modified and its permanent attachment to an artificial linker can affect cell viability for subsequent analysis. Hence, affinity-based sorting of CTCs can limit their clinical applications and subsequent characterizations.

In contrast, in label-free CTC sorting methods distinct physical properties, such as size, shape, deformability, adhesion, compressibility, polarizability, and magnetic susceptibility are determining [11–14]. These methods can help to resolve the limitations of the affinity-based methods. For example, they can achieve intact CTC capturing without influencing cell viability. In addition, viable and intact CTCs are compatible with the downstream clinical analysis [15]. These high viability and purity of captured CTCs are essential for gaining precise cancer information using genetic technologies [16–18]. In spite of their benefits, label-free CTC sorting methods have some limitations too. For instance, many types of CTCs, have similar physical properties (e.g. size and shape) to white blood cells (WBCs) [19, 20], thus leading to a significant WBC contamination in the isolated CTC samples [21].

Dielectrophoresis (DEP) is a physical phenomenon observed when microparticles and cells are exposed to electric field gradient. DEP has been applied in various forms on a diverse set of biomolecules and particles including proteins, exosomes, bacteria, yeast, stem cells, cancer cells, and blood cells to manipulate and analyze their behaviors [22]. One of the most frequent applications of DEP is discrimination and separation of cells and particles based on their different dielectric properties and sizes [23–25]. For instance, Alazzam *et al* has used DEP to separate MDA-231 (human breast cancer) cells from blood-based on their different crossover frequency [26]. They separated cancer and normal cells and collected them in two different outlets. In a similar work, Alshareef *et al* used DEP for the separation of MCF-7 (human breast cancer) cells and HCT-116 (human colorectal carcinoma) cells [27]. Modarres *et al*, used two different frequencies, as release and capture frequencies, to separate polystyrene particles based on their sizes and then, investigated the feasibility of their method for separation of MCF-7 cells from red blood cells [28]. One strength of the DEP is providing the possibility of performing various on-chip downstream analysis on the cells without a need to collecting the cells in the output. In fact, using DEP, cells can be kept fixed even in presence of moving flows, and one can perform different experiments with them by exchanging a low volume of different reagents. Here, we have introduced a thin PDMS porous membrane to hold the CTCs trapped by the DEP within its micropores at a single-cell level for downstream biological analysis.

Microwells have been utilized widely for trapping precise quantities of particles and cells, in particular single cells. Various methods have been introduced for the fabrication of microwells including biochemical patterning, direct printing, microfluidic methods, and laser sintering processes. The most frequent method in microwell fabrication is photolithography [29, 30]. This process may involve some challenges and limitations. Firstly, photolithography method has a low production rate. Furthermore, in some cases, it needs an aligner system to align different layers of the device together through the process. Moreover, microwells may not be dug completely due to various reasons like an insufficient exposure or an imperfect developing procedure. In exposure, different factors including intensity and time are influential, and if one of these factors is nonoptimal, we do not achieve the desired fabrication result. In addition, diffraction is a typical phenomenon in photolithography, especially in thick transparent resist layers which may cause a defective lithography. Hence, these undesired effects may result in an extra layer of resist remain on the surface of the electrodes inside the wells which will influence the trapping efficiency. Consequently, we are obligated to replace the device completely as it does not perform well.

In the device proposed here, we use an array of SU-8 micropillars and soft lithography process to fabricate a replaceable porous PDMS membrane for trapping CTCs. There are different dimensions of pillars on the SU-8 mold and it can be used several times for building different sizes of pores for various goals. In addition, here, we do not come across the challenges mentioned above for previous fabrication procedures of microwells. Micropores are completely dug using SU-8 pillars. Furthermore, there is no need for an aligner to align the microwells on top of the electrodes since we can quite easily shift the membrane under an optical microscope to find the best alignment, and, the membrane can be easily replaced with no additional device alteration in the case of deficiencies.

2. Design of the microfluidic device

The proposed microfluidic device consists of a few components located inside a PDMS channel. The channel height is 80 μm. The gold interdigitated electrodes are fabricated on the surface of a glass slide and the distance between two adjacent electrodes is around 10–15 μm. These electrodes are used to apply positive DEP on CTCs. A PDMS porous membrane is positioned on top of the surface of the electrodes so that in an ideal situation, in every single micropore there are two adjacent electrodes. The micropores which act as cell traps have a diameter of 20–30 μm, selected based on the size of CTCs. The height of the membrane is roughly 30 μm. Figure 1(a) shows a schematic view of the chip. Cells enter the channel and are trapped inside the micropores by positive DEP after setting the flow rate, frequency, and amplitude of the signal. Figure 1(b) shows the side-view of a single micropore including its dimensions.

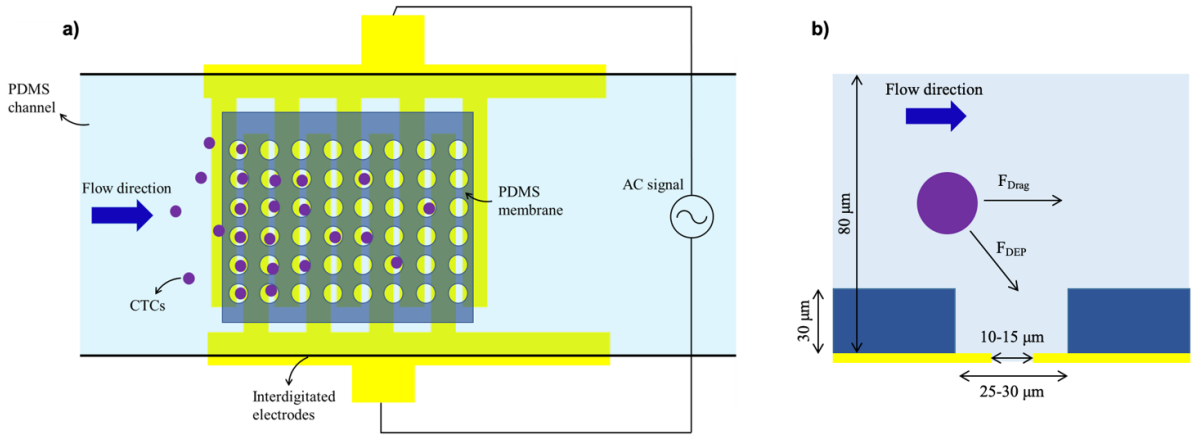

Figure 1. Schematic view of the microfluidic chip. (a) Structure of the device and its trapping function. Cells are entered into the device from the left side and then trapped inside the micropores by positive DEP force. (b) Side-view of a single micropore showing the main forces exerted on a cell.

3. Theory

3.1. DEP

DEP is the movement of a neutral particle in a non-uniform electric field due to the interaction of the particle's dipole moment with the spatial gradient of the electric field. DEP has been extensively used in many microfluidic applications and it is instrumental in manipulating particles and cells at microscales due to its desirable scaling for the systems of the reduced size. The time averaged dielectrophoretic force can be approximated in terms of the electric dipole moments as:

$$\langle F_{\mathrm{DEP}}(t)\rangle = 2\pi\varepsilon_m [f_{\mathrm{CM}}] R^3 \nabla E_{\mathrm{rms}}^2 \tag{1}$$

where ε_m is the relative permittivity of the medium, R is the particle radius, E_{rms} is the root-mean-square magnitude of the applied AC electric field. $[f_{\mathrm{CM}}]$ is the real part of Clausius–Mossotti (CM) factor relating to the induced dipole moment as the following,

$$f_{\mathrm{CM}}(\tilde{\varepsilon}_p, \tilde{\varepsilon}_m) = \frac{\tilde{\varepsilon}_p - \tilde{\varepsilon}_m}{\tilde{\varepsilon}_p + 2\tilde{\varepsilon}_m} \tag{2}$$

and,

$$\tilde{\varepsilon} = \varepsilon - j\left(\frac{\sigma}{\omega}\right) \tag{3}$$

where $\tilde{\varepsilon}$ is the complex permittivity. Now f_{CM} can be rewritten as,

$$f_{\mathrm{CM}}(\varepsilon_p, \varepsilon_m, \sigma_p, \sigma_m, \omega) = \frac{(\varepsilon_p - \varepsilon_m) + \frac{j}{\omega}(\sigma_p - \sigma_m)}{(\varepsilon_p + 2\varepsilon_m) + \frac{j}{\omega}(\sigma_p + 2\sigma_m)} \tag{4}$$

where ε_p is the relative permittivity of the particle, σ_p is the electrical conductivity of the particle, and σ_m is the electrical conductivity of the medium.

Dielectrophoretic force depends on the sign and the magnitude of the CM factor, f_{CM}. If $f_{\mathrm{CM}} > 0$, then the particles will be attracted toward the electric field strength maxima; this is called positive DEP (p-DEP). Otherwise, the particles will be repelled from the electric field strength maxima, which is called negative DEP (n-DEP) [31–34].

3.2. Drag force

At the creeping-flow limit known as Stokes' law, a floating spherical particle in a fluidic channel experiences a drag force defined as,

$$F_{\mathrm{Drag}} = 6\pi\mu R(u - u_p) \tag{5}$$

where R is the particle radius, u is the fluid velocity, u_p is the particle velocity, and μ is the viscosity of the fluid [34, 35].

4. Simulation

The trajectory of a particle inside the microchannel is a result of its interaction with the surrounding fields, consequently, corresponding field variables need to be carefully specified. For the DEP applications in microfluidics, the electric field, the flow field, and the temperature field (if considerable temperature gradient present) need to be considered [34]. Here, we used the finite element method (FEM) method in COMSOL Multiphysics 5.4 to simulate the function of the device. The laminar flow, electric current and particle tracing for fluid flow physics were included in stationary, frequency domain and time dependent studies, respectively. All the simulation parameters are listed in table 1.

Two fields are assumed in our simulation, the electric field, and the flow field, hence, there are two main forces applied to the cells, the dielectrophoretic force and the drag force. Although the cells' trajectories are derived by the total force, another important parameter contributing in capturing the cells into the pores is the channel height which needs to be carefully selected. If the height of the channel is too small, most of the cells are pulled down to the first rows of the pores by the positive DEP and result in cell accumulation in the channel (figure 2(a)). In contrast, if the height of the channel is too large, most of the cells are led to the output by the drag

Table 1. List of the simulation parameters (cancer and normal cells dielectric properties can be found in [36]).

Parameter	Value	Parameter	Value
Medium conductivity (σ_m)	10^{-3} (s m^{-1})	Dynamic viscosity of medium	10^{-3} (Pa s^{-1})
Gold electrodes conductivity	42.55×10^6 (s m^{-1})	Electrodes gap	10 (μm)
PDMS conductivity	10^{-5} (s m^{-1})	Frequency of signal	3 (MHz)
Medium density	1000 (kg m^{-3})	Channel height	80 (μm)
Relative permittivity of medium (ε_m)	80	Membrane thickness	30 (μm)
Relative permittivity of PDMS	2.75	Voltage amplitude	14 ($V_{p\text{-}p}$)
Relative permittivity of gold	30	Initial flow rate	35 (μm s^{-1})

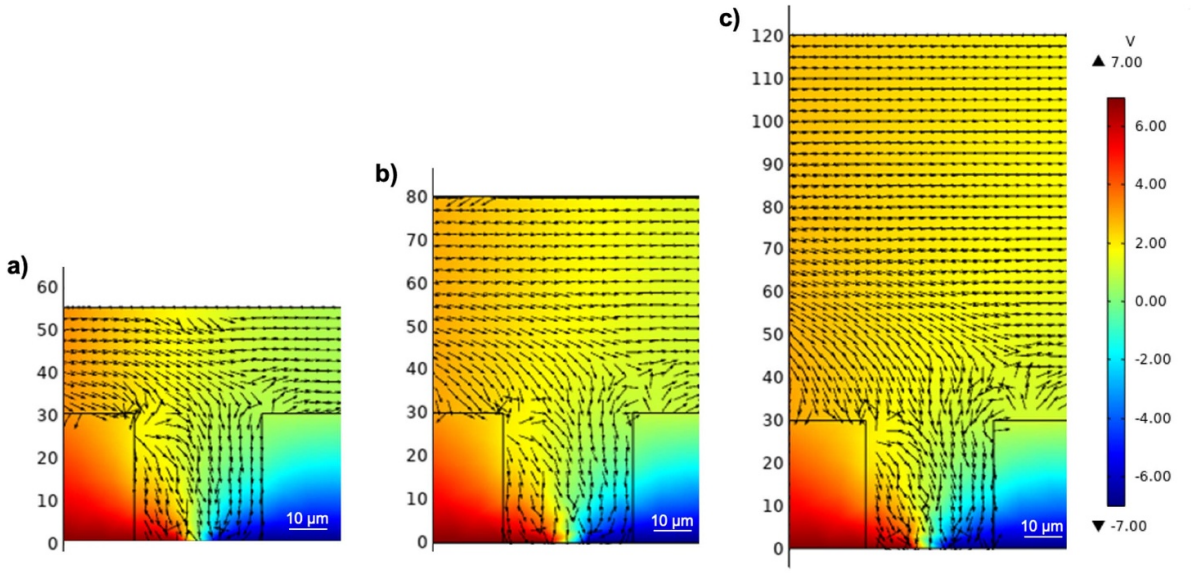

Figure 2. Side-view of the total force contour lines applied to the cells on the top of a pore for different heights of the microchannel (a) 55 μm, (b) 80 μm, and (c) 120 μm.

force as it dominates around the upper height of the channel (figure 2(c)). The simulation results suggest that around the height of 80 μm, with voltage amplitude of 14 $V_{p\text{-}p}$ and initial flow rate of 35 μm s^{-1}, there is a good balance between these two forces (figure 2(b)), and therefore we designed our microchannel to work around this height.

Based on equation (1), the dielectrophoretic force is associated with the gradient of the electric field. Figure 3(a) shows the logarithmic gradient of the electric field, i.e. ∇E_{rms}^2, for the voltage of 14 $V_{p\text{-}p}$, in a micropore. It is clearly seen that the gradient of the electric field is maximal around the edges of the electrodes. As a result, dielectrophoretic force is maximal inside the pores having two adjacent electrodes underneath.

For the drag force, the flow rate is determining. Per equation (5), by increasing the flow rate, the drag force increases and finally overcomes the dielectrophoretic force, therefore guides cells toward the outlet which finally results in lower trapping efficiency. In contrast, at low flow rates particles will accumulate in one location and do not advance to the top of the pores. This suggests that choosing the right flow rate is vital for having a good trapping efficiency. In figures 3(b) and (c), we can see a side-view of the total force applied to cells on the top of a pore at two different initial flow rates (35 μm s^{-1} and 105 μm s^{-1}). It is obvious that by increasing the flow rate, most of the force contour lines push cells toward the channel output. Figure 3(d) demonstrates that in an optimal situation (after setting the flow rate and the voltage amplitude), the total force contour lines explicitly guide cells toward the electrodes and thus to the inside of the pores (surface color shows the logarithmic magnitude of the electric field).

5. Materials and methods

5.1. Fabrication of the microfluidic chip

The fabrication of the chip consists of three major steps: (a) fabrication of the porous membrane, (b) preparing the substrate and patterning the electrodes on it, and (c) fabrication of the microfluidic channel and finally assembling these components.

For the fabrication of the porous membrane, we used the soft lithography process. The membrane has an approximate thickness of 30 μm and consists of an array of micropores for trapping the cells. We used a mold and a sacrificial layer for making it. The fabrication process is outlined in figure 4. First, we made a SU-8 mold in order to form the pores inside the membrane. A silicon wafer was cleaned using acetone, isopropyl alcohol (IPA), and deionized (DI) water,

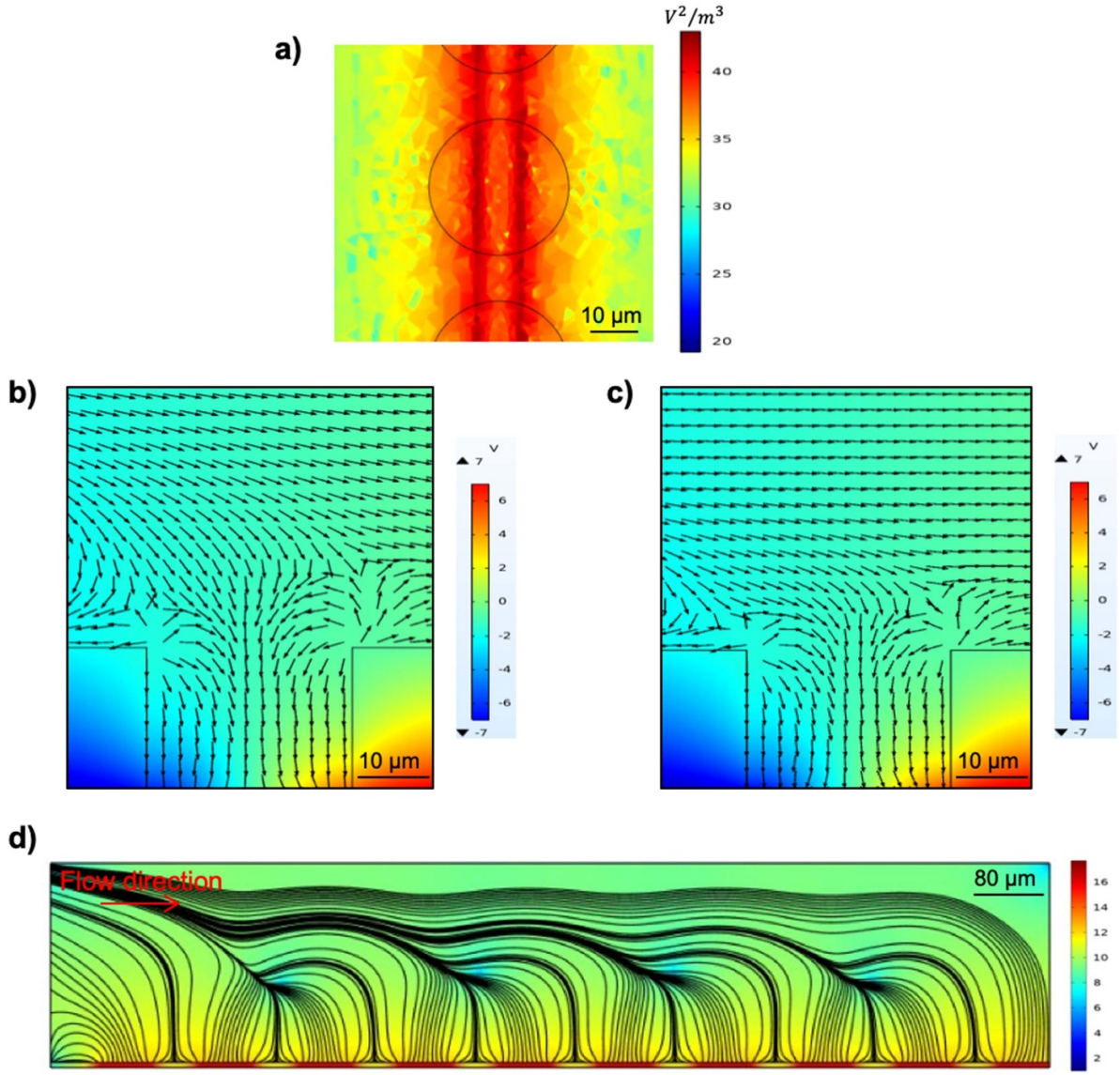

Figure 3. Simulation results for the medium conductivity (σ_m) of 10^{-3} (s m^{-1}), the electrode gap of 10 μm, the membrane thickness of 30 μm, and the channel height of 80 μm. (a) Logarithmic gradient of the electric field (indicative of the DEP force) at the bottom of a pore for the applied voltage of 14 $V_{p\text{-}p}$. The field is maximum around the edges of the electrodes. (b) Side-view of the total force contour lines applied to cells on the top of a pore for the applied voltage of 14 $V_{p\text{-}p}$ and at the optimal initial flow rate of 35 μm s^{-1} (guiding cells into the pore). (c) Side-view of the total force contour lines applied to cells on the top of a pore for the voltage of 14 $V_{p\text{-}p}$ and at 3$\times$ of the optimal initial flow rate, i.e. 105 μm s^{-1} (leading cells toward the outlet). (d) Side-view of the total force contour lines along the channel for the optimal situation showing the routes in which cells move toward the electrodes for the voltage of 14 $V_{p\text{-}p}$ and the flow rate of 35 μm s^{-1} (surface color is the logarithmic magnitude of the electric field).

then coated with SU-8 2050 photoresist (MicroChem, Newton, MA, USA). The layer's height was chosen to be roughly 45 μm (spinning at 2500 rpm for 1 min). After prebaking at 100 °C for 20 min, the layer was patterned using direct laser lithography (μPG101, Heidelberg, Germany) to make the pillar array. After a post-exposure bake step (100 °C for 20 min) the structure was developed and hard baked at 160 °C for 10 min. Figure 5(a) shows the scanning electron microscope (SEM) image of the fabricated mold. For making the membrane, a thin layer of polyvinyl alcohol was coated on top of the mold using spin coater. This layer is the sacrificial layer and later will be removed. Next, a 20–30 μm thick polydimethylsiloxane (PDMS), (Sylgard 184, Dow Corning, Midland, MI, USA) layer was coated on the sacrificial layer to form the membrane. After baking the PDMS at 80 °C for 1 h, this solid layer was immersed inside the DI water for 1 h to dissolve the alcohol layer. Finally, the membrane was simply detached from the mold. For transferring the PDMS membrane onto the electrodes' surface, first, it was floated in DI water and then the glass substrate coated with electrodes came in contact with the membrane from below. The membrane position was adjusted under a microscope and finally, the whole assembly heated on a hot plate for attachment [37]. Figure 5(b) shows the SEM image of the fabricated membrane.

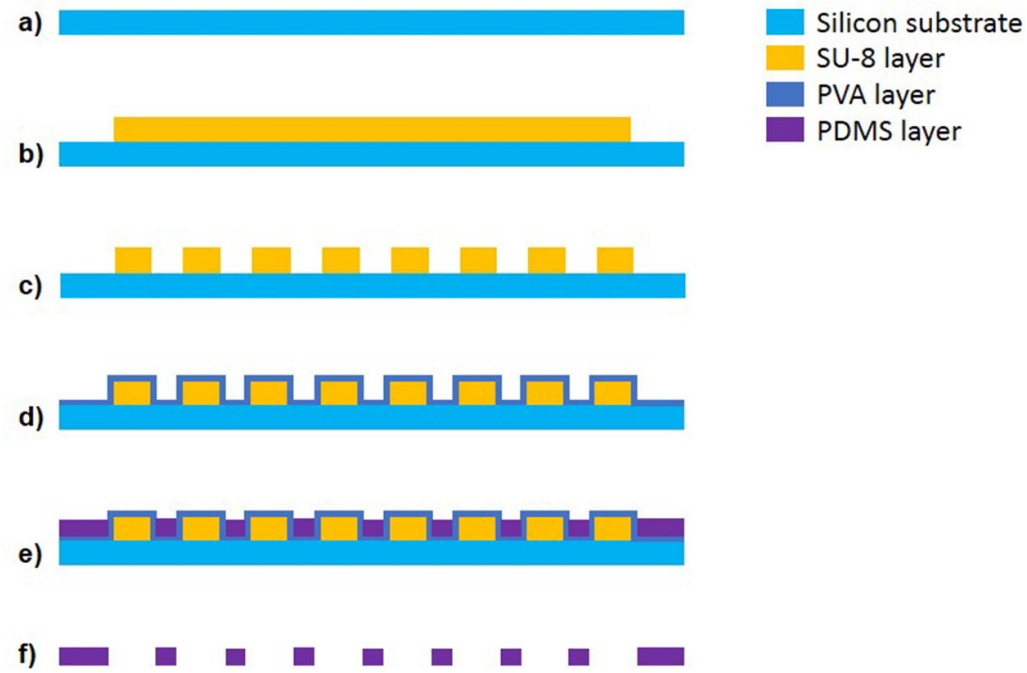

Figure 4. Fabrication process of the PDMS membrane. (a) Rinsing the silicon substrate, (b) coating the substrate with the SU-8 photoresist layer, (c) patterning the SU-8 pillars by the direct laser lithography, (d) coating the pillars with a thin alcohol layer (PVA), (e) pouring and spinning the PDMS on the SU-8 pillars, and (f) peeling off the final membrane from the mold.

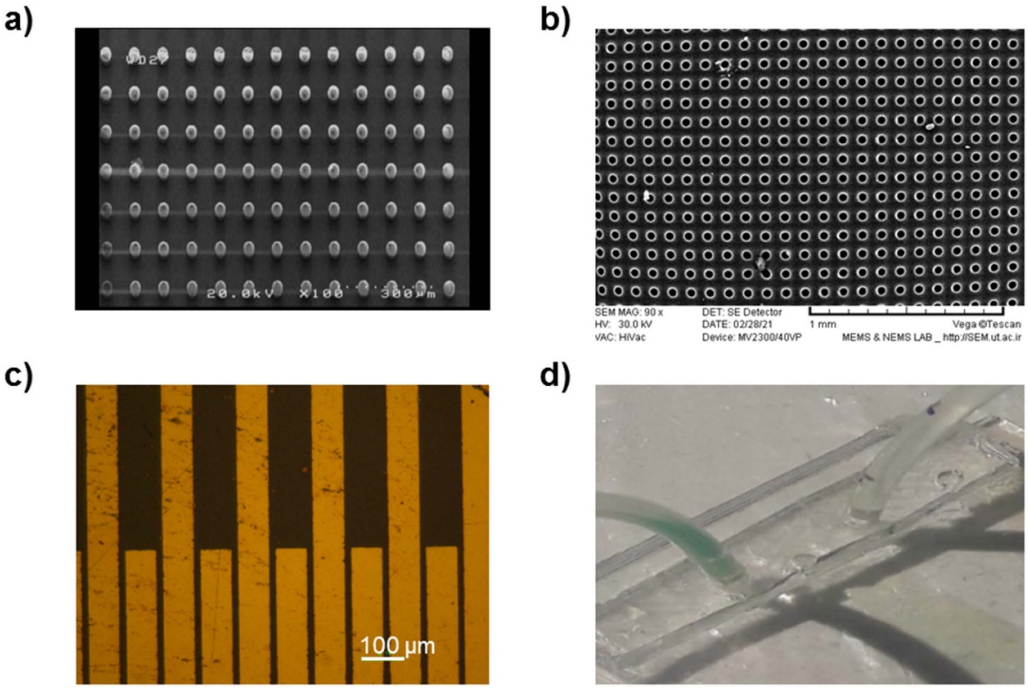

Figure 5. Fabrication results. (a) The SEM image of the SU-8 pillar array on the mold, (b) the SEM image of the PDMS porous membrane, (c) the gold interdigitated electrodes, and (d) the microfluidic channel.

Gold electrodes were made using photolithography process on a glass substrate. First, after washing the glass slide in acetone, IPA, and DI water, a thin layer of Ti-Au (Ti: 30 nm and Au: 200 nm) was deposited on the glass using Radio Frequency (RF) sputtering. The electrodes were then patterned using Shipley photoresist S1813 (MicroChem, Newton, MA, USA) by direct laser lithography (μPG101, Heidelberg, Germany). Finally, after developing the photoresist, the electrodes were etched using Au etchant [HCL (37%), HNO_3 (60%)—3:1], and then they were passivated by a 2–3 μm layer of diluted SU-8. Figure 5(c) shows the image of the interdigitated gold electrodes on the glass slide.

For making the microfluidic channel, we used PDMS. An 80 μm thick SU-8 mold for the channel was first patterned using the photolithography, then, after pouring the PDMS on it, we baked it for 1 h at 80 °C and then peeled it off from the substrate.

After rinsing the membrane and electrodes' surface with alcohol, we placed the membrane on top of the electrodes and aligned the position, then we put them inside an oven at 80 °C for 20 min. Finally, for bonding the PDMS channel to the electrodes surface, the PDMS channel and the glass slide were treated in oxygen plasma for 1 min. The channel was bound to the glass slide using hand pressure and baked for 20 min at 80 °C. Figure 5(d) shows the fabricated microfluidic channel.

5.2. Cell culture and sample preparation

PC3 cells (human prostate cancer cell line) were obtained from a standard cell bank. The flask was kept in an incubator (5% CO2, 95% air) at 37 °C in Dulbecco's Modified Eagle's Medium (DMEM) supplemented with 10% fetal bovine serum, and 1% penicillin/streptomycin. After three days, cultured cells were detached from the bottom of the flask using 1 ml of trypsin. After adding 3 ml of growth medium, the falcon is centrifuged for 5 min at 1500 rpm. Finally, cells were suspended into a DEP buffer (10% sucrose (w/v), 0.5% dextrose (w/v) in DI water). All the cell culture materials are from Gibco (Thermo Fisher Scientific, Waltham, MA, USA).

6. Results and discussion

6.1. DEP effects on the cells

Applying DEP on live cells can theoretically end in two major effects: Joule heating and direct cell-field interaction.

Applying an electric field to a conductive suspension leads to power dissipation in the form of Joule heating. Hence, if the resulted temperature change is greater than a few degrees Celsius, it can cause some effects on the cell physiology phenotype. Archer *et al* showed that after a 15 min exposure to the electric field created with a voltage of 21 $V_{p\text{-}p}$ and in a medium with a conductivity of 10 ms m^{-1}, the overall steady-state temperature rise was just around 1 °C [38]. Although not so harmful to the cells, this minimal temperature fluctuation can possibly lead to the upregulation of heat shock proteins. It has been found that the current induced heating is proportional to the medium conductivity, thus, a relatively low conductivity is preferred to minimize temperature excursion and its destructive effects. In this work, we used DEP buffer having a conductivity of around 10 ms m^{-1} to prevent induced heating.

Another possible damage is the membrane rupture due to high transmembrane voltage. The membrane of the cell may be hurt if transmembrane potential (induced by the electric field) overpasses the membrane dielectric breakdown voltage. Acceptable threshold potential for cancer cells' membrane is around 1 V. Again, as Archer *et al* reported by increasing the frequency, the induced membrane potential will decrease [38]. For example, at a frequency of 5 MHz for a voltage amplitude of 21 $V_{p\text{-}p}$ and in a medium conductivity of 10 ms m^{-1}, they measured the potential difference across the cell membrane to be in the range of 8.6–68 $\mu V_{p\text{-}p}$. In contrast, at lower frequencies the membrane potential is higher, approaching 5 $V_{p\text{-}p}$, a value that is enough to rupture cellular membranes. Consequently, in this work, we have selected a frequency of 6 MHz to prevent cell membrane rupture. Besides, this frequency can help us to avoid bubble formation and electrode polarization.

The extent of genetic transformation that a living cell experiences while subjected to an electric field is not certain and one major benefit of using DEP is that the cells do not suffer major genetic dysregulation. An important factor in the genes transformation is the duration of the field exertion. In other words, longer DEP applications may have a higher impact on the cells. Earlier studies have shown that an exposure of 15 min does not have a major effect on the cells' phenotype. The present investigation carries out DEP for a very short time. The cells are trapped in about two minutes and any subsequent experiment with the cells can happen almost immediately. Moreover, most of the studies that report high stress exerted on cells are with the applied frequency close to the cells crossover frequency, i.e. 23 KHz. Here, our working frequency is far higher, i.e. 6 MHz, to keep the cells immune against the exerted electric field [38–43].

6.2. Experimental setup

To evaluate the performance of the device, as mentioned above, we used cultured prostate cancer cells as CTC model. First, the microfluidic channel was rinsed with PBS buffer and then placed under a microscope with an installed camera (DS-Fi2, Nikon, Tokyo, Japan) to monitor movements of cancer cells. The channel inlet and outlet were connected to a syringe pump (TS-1B, LongerPump, Hebei, China) using feeder tubes to supply the optimal flow rate. To apply DEP on cells, platinum wires were used to connect the interdigitated gold electrodes to a function generator. Finally, all the measurement parameters were experimentally optimized for the highest cell trapping.

6.3. Trapping the cells

The performance of the device was examined in two steps. First, we assessed the effect of the DEP force without the membrane being present. We swept the frequencies and the voltage amplitudes to find the optimal parameters for higher trapping. Cells started being trapped at the voltage of 2 $V_{p\text{-}p}$ and the frequency of 6 MHz. In the next step, we evaluated the performance of the actual device including the PDMS membrane. The voltage amplitude of 14 $V_{p\text{-}p}$ and the frequency of 6 MHz exhibited the desired result. The flow rate was set at 3 μl min^{-1}. After injecting the cells into the channel, p-DEP is exerted on the cells and attracts them toward the edges of the electrodes into the micropores, where the gradient of the electric field is maximum. It is to be noted that PC3 cells have an average size of 22 μm, and the pores are 30 μm. Figure 6(a)

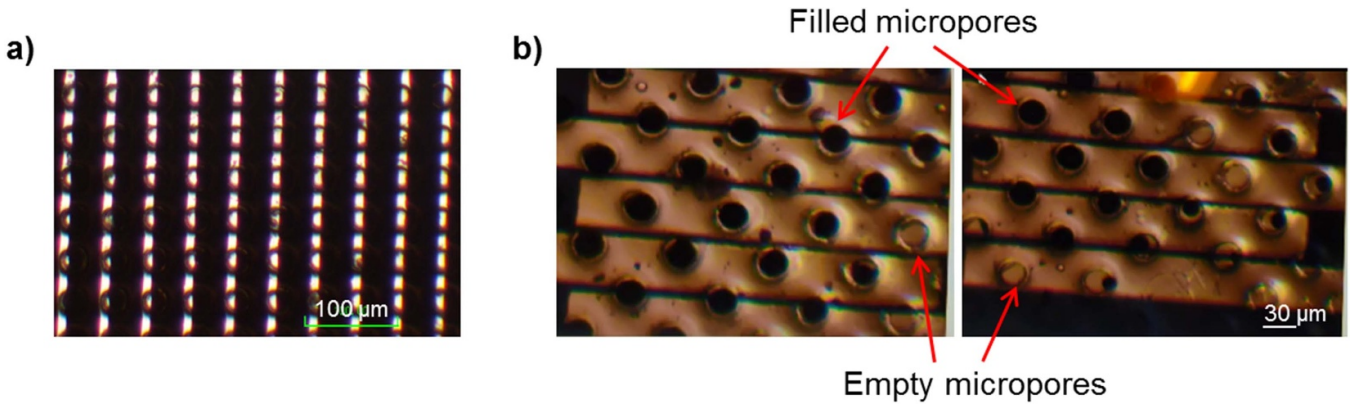

Figure 6. Microfluidic chip and cell trapping with DEP. (a) Final fabricated device where dark rows are the electrodes with the micropores seen in between, (b) trapped cancer cells inside the micropores.

shows the final microfluidic chip illuminated from the bottom. Electrodes are dark and the pores in between are bright. As seen from figure 6(b), the cancer cells have been trapped considerably within the micropores, they are almost fixed and ready for further biological analysis.

7. Conclusion

Here we introduced a microfluidic chip for trapping CTCs in PDMS micropores using the DEP phenomenon and used cultured cancer cells (PC3) as a model for CTCs to test the feasibility of trapping. The dielectrophoretic force is induced by the gold electrodes patterned on the glass substrate underneath the porous membrane and works based on the size and dielectric properties of the target cells so that larger cells experience stronger force. The proposed device enables us to efficiently trap single cells inside the micropores and hold them fixed for subsequent biological analysis such as immunostaining, viability/apoptosis assay, and fluorescent *in situ* hybridization. All these assays are readily being performed by sequentially injecting reagents to the pores embedding the single cells without the need for complicated valve or tubing systems. The porous membrane used in this device can be replaced with a new one having different features without sacrificing the whole chip performance. Moreover, the device fabrication process was quite simple without facing the challenges involved in the photolithography or otherwise in aligning the microwells to the substrate electrodes.

Data availability statement

No new data were created or analyzed in this study.

Acknowledgments

The authors also acknowledge the contribution of Mohsen Mashhadi Kashtiban during the investigation phase of the project.

ORCID iDs

Malihe Farasat https://orcid.org/0000-0003-2306-9708
Atin Bakhshi https://orcid.org/0000-0002-8718-7212
Majid Badieirostami https://orcid.org/0000-0002-1647-7052

References

[1] Yu M, Stott S, Toner M, Maheswaran S and Haber D A 2011 Circulating tumor cells: approaches to isolation and characterization *J. Cell Biol.* **192** 373–82
[2] Kim S H *et al* 2011 Electroactive microwell arrays for highly efficient single-cell trapping and analysis *Small* **7** 3239–47
[3] Kobayashi M, Kim S H, Nakamura H, Kaneda S and Fujii T 2015 Cancer cell analyses at the single cell-level using electroactive microwell array device *PLoS One* **10** e0139980
[4] Krebs M G, Hou J-M, Ward T H, Blackhall F H and Dive C 2010 Circulating tumour cells: their utility in cancer management and predicting outcomes *Ther. Adv. Med. Oncol.* **2** 351–65
[5] Nagrath S *et al* 2007 Isolation of rare circulating tumour cells in cancer patients by microchip technology *Nature* **450** 1235–9
[6] Tan S J, Yobas L, Lee G Y H, Ong C N and Lim C T 2009 Microdevice for the isolation and enumeration of cancer cells from blood *Biomed. Microdevices* **11** 883–92
[7] Augustsson P, Magnusson C, Nordin M, Lilja H and Laurell T 2012 Microfluidic, label-free enrichment of prostate cancer cells in blood based on acoustophoresis *Anal. Chem.* **84** 7954–62
[8] Antfolk M, Antfolk C, Lilja H, Laurell T and Augustsson P 2015 A single inlet two-stage acoustophoresis chip enabling tumor cell enrichment from white blood cells *Lab Chip* **15** 2102–9
[9] Li P *et al* 2015 Acoustic separation of circulating tumor cells *Proc. Natl Acad. Sci.* **112** 4970–5
[10] Lindsay C R *et al* 2019 EPAC-lung: pooled analysis of circulating tumour cells in advanced non-small cell lung cancer *Eur. J. Cancer* **117** 60–68
[11] Gossett D R, Weaver W M, Mach A J, Hur S C, Tse H T K, Lee W, Amini H and Di Carlo D 2010 Label-free cell separation and sorting in microfluidic systems *Anal. Bioanal. Chem.* **397** 3249–67

[12] Holm S H, Beech J P, Barrett M P and Tegenfeldt J O 2011 Separation of parasites from human blood using deterministic lateral displacement *Lab Chip* **11** 1326–32
[13] Sollier E *et al* 2014 Size-selective collection of circulating tumor cells using Vortex technology *Lab Chip* **14** 63–77
[14] Fallahi H, Zhang J, Phan H-P and Nguyen N-T 2019 Flexible microfluidics: fundamentals, recent developments, and applications *Micromachines* **10** 830
[15] Che J *et al* 2016 Classification of large circulating tumor cells isolated with ultra-high throughput microfluidic Vortex technology *Oncotarget* **7** 12748
[16] Yeo T *et al* 2016 Microfluidic enrichment for the single cell analysis of circulating tumor cells *Sci. Rep.* **6** 1–12
[17] Thompson A *et al* 2014 Microfluidics for single-cell genetic analysis *Lab Chip* **14** 3135–42
[18] Khamenehfar A *et al* 2016 Dielectrophoretic microfluidic chip enables single-cell measurements for multidrug resistance in heterogeneous acute myeloid leukemia patient samples *Anal. Chem.* **88** 5680–8
[19] Allard W J, Tibbe A G J, Uhr J W and Terstappen L W M M 2004 Tumor cells circulate in the peripheral blood of all major carcinomas but not in healthy subjects or patients with nonmalignant diseases *Clin. Cancer Res.* **10** 6897–904
[20] Marrinucci D *et al* 2010 Cytomorphology of circulating colorectal tumor cells: a small case series *J. Oncol.* **2010** 1–7
[21] Zhu S, Jiang F, Han Y, Xiang N and Ni Z 2020 Microfluidics for label-free sorting of rare circulating tumor cells *Analyst* **145** 7103–24
[22] Sarno B, Heineck D, Heller M J and Ibsen S D 2021 Dielectrophoresis: developments and applications from 2010 to 2020 *Electrophoresis* **42** 539–64
[23] Li M and Anand R K 2017 High-throughput selective capture of single circulating tumor cells by dielectrophoresis at a wireless electrode array *J. Am. Chem. Soc.* **139** 8950–9
[24] Hunt T P, Issadore D and Westervelt R M 2008 Integrated circuit/microfluidic chip to programmably trap and move cells and droplets with dielectrophoresis *Lab Chip* **8** 81–87
[25] Kim S H, He X, Kaneda S, Kawada J, Fourmy D, Noji H and Fujii T 2014 Quantifying genetically inserted fluorescent protein in single iPS cells to monitor Nanog expression using electroactive microchamber arrays *Lab Chip* **14** 730–6
[26] Alazzam A, Stiharu I, Bhat R and Meguerditchian A-N 2011 Interdigitated comb-like electrodes for continuous separation of malignant cells from blood using dielectrophoresis *Electrophoresis* **32** 1327–36
[27] Alshareef M, Metrakos N, Juarez Perez E, Azer F, Yang F, Yang X and Wang G 2013 Separation of tumor cells with dielectrophoresis-based microfluidic chip *Biomicrofluidics* **7** 011803
[28] Modarres P and Tabrizian M 2019 Frequency hopping dielectrophoresis as a new approach for microscale particle and cell enrichment *Sens. Actuators* B **286** 493–500
[29] Kim S H, Yamamoto T, Fourmy D and Fujii T 2011 An electroactive microwell array for trapping and lysing single-bacterial cells *Biomicrofluidics* **5** 024114
[30] Morimoto A *et al* 2015 High-density dielectrophoretic microwell array for detection, capture, and single-cell analysis of rare tumor cells in peripheral blood *PLoS One* **10** e0130418
[31] Wanichapichart P, Bunthawin S, Kaewpaiboon A and Kanchanapoom K 2002 Determination of cell dielectric properties using dielectrophoretic technique *ScienceAsia* **28** 113–9
[32] Voldman J 2006 *Dielectrophoretic Traps for Cell Manipulation, in BioMEMS and Biomedical Nanotechnology* (Berlin: Springer) pp 159–86
[33] Zhang C, Khoshmanesh K, Mitchell A and Kalantar-zadeh K 2010 Dielectrophoresis for manipulation of micro/nano particles in microfluidic systems *Anal. Bioanal. Chem.* **396** 401–20
[34] Çetin B and Li D 2011 Dielectrophoresis in microfluidics technology *Electrophoresis* **32** 2410–27
[35] Leal L G 2007 *Advanced Transport Phenomena: Fluid Mechanics and Convective Transport Processes* vol 7 (Cambridge: Cambridge University Press)
[36] Polevaya Y, Ermolina I, Schlesinger M, Ginzburg B-Z and Feldman Y 1999 Time domain dielectric spectroscopy study of human cells: II. Normal and malignant white blood cells *Biochim. Biophys. Acta (BBA)-Biomembr.* **1419** 257–71
[37] Mashhadi Kashtiban M *et al* 2019 Design, numerical analysis and fabrication of PDMS porous membrane for medical applications (ISME) (available at: www.researchgate.net/publication/333145664_trahythlyl_ddy_w_sakht_ghsha_mtkhlkhl_bh_mnzwr_karbrdhay_pzshky/references)
[38] Archer S, Li -T-T, Evans A T, Britland S T and Morgan H 1999 Cell reactions to dielectrophoretic manipulation *Biochem. Biophys. Res. Commun.* **257** 687–98
[39] Nerguizian V, Stiharu I, Al-Azzam N, Yassine-Diab B and Alazzam A 2019 The effect of dielectrophoresis on living cells: crossover frequencies and deregulation in gene expression *Analyst* **144** 3853–60
[40] Huang C, Liu C, Loo J, Stakenborg T and Lagae L 2014 Single cell viability observation in cell dielectrophoretic trapping on a microchip *Appl. Phys. Lett.* **104** 013703
[41] Huang Y, Joo S, Duhon M, Heller M, Wallace B and Xu X 2002 Dielectrophoretic cell separation and gene expression profiling on microelectronic chip arrays *Anal. Chem.* **74** 3362–71
[42] Yoshioka J, Yoshitomi T, Yasukawa T and Yoshimoto K 2016 Alternation of gene expression levels in mesenchymal stem cells by applying positive dielectrophoresis *Anal. Sci.* **32** 1213–6
[43] Menachery A and Pethig R 2005 Controlling cell destruction using dielectrophoretic forces *IEE Proc. Nanobiotechnol.* **152** 145